The College of Engineering
University of Wisconsin-Madison

Wisconsin Electric Machines and Power Electronics Consortium

RESEARCH REPORT
88-6

Core Loss in Buried Magnet Permanent Magnet Synchronous Motors

Rich Schiferl and T.A. Lipo
Department of Electrical & Computer Engineering
University of Wisconsin-Madison
1415 Johnson Drive
Madison, WI 53706-1691

WEMPEC

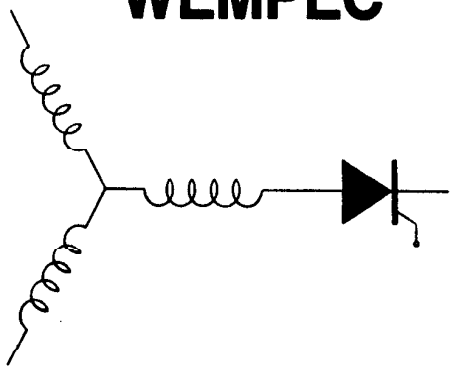

Department of Electrical and Computer Engineering
1415 Johnson Drive
Madison, Wisconsin 53706

CORE LOSS IN BURIED MAGNET PERMANENT MAGNET SYNCHRONOUS MOTORS

Rich Schiferl, Member, IEEE T.A. Lipo, Fellow, IEEE
University of Wisconsin
Department of Electrical and Computer Engineering
Madison, Wisconsin 53706-1691

Abstract

The steady state core loss characteristics of buried magnet, synchronous motors operating from a sinusoidal, constant frequency voltage supply are investigated. Measured and calculated core loss, with constant shaft load, is shown to increase with decreasing terminal voltage due to an increase in armature reaction induced stator flux density time harmonics. Finite element modeling is used to show that the additional loss due to stator core flux density time harmonic fields may increase core loss by a factor of six over the loss associated with only the fundamental component field at low motor flux levels. A simple air gap model of motor flux components shows that this increased loss is due to localized rotor saturation.

INTRODUCTION

Permanent magnets have been employed as an alternative to current carrying coils for magnetic field excitation in synchronous machines for over 30 years. The lack of slip rings, brushes and field winding losses have always been viewed as distinct advantages over that of conventional, wound field machines. Early applications included the use of Alnico magnets in small generators[1]. More recently, with the advent of improved ferrite and rare earth magnets and the parallel impact of the "energy crisis" of the past decade, there has been a renewed interest in permanent magnet synchronous machine development for mass market applications. In particular, a large body of research was devoted to the analysis and design of line start permanent magnet synchronous motors in the late 1970's and in the 1980's [2-9]. In these machines the magnets are buried below a rotor squirrel cage winding which, as in an induction motor, lies in slots near the air gap as shown in the one pole cross section in Figure 1. The squirrel cage carries current only during starting since steady state operation is at synchronous speed thereby eliminating all steady state rotor I^2R losses which are naturally present in an induction motor. This elimination of rotor conductor loss coupled with a reduced requirement of armature magnetizing current and its associated copper loss was the main impetus for proposing the buried magnet, line start motor as a replacement for high efficiency induction motors in low power applications (two to 25 horsepower). Many prototype permanent magnet motors of this type were built and at least one such motor reached the market in the 1970's [2].

Although the advantages of reduced I^2R loss in permanent magnet synchronous motors is clear, core loss comparisons between these motors and induction motors are more cloudy. Steady state core loss is largely a function of the harmonic content of the core flux density. Unlike induction motors, the air gap flux of a buried magnet motor may be very nonsinusoidal due to the combination of magnet flux harmonics as well as the interaction of armature MMF with the complicated rotor magnetic structure. In [10] it was shown that these harmonic fields had a significant influence on stator core loss in salient pole surface magnet motors but no qualitative or quantitative description of their effects on core loss in buried magnet motors has yet been published.

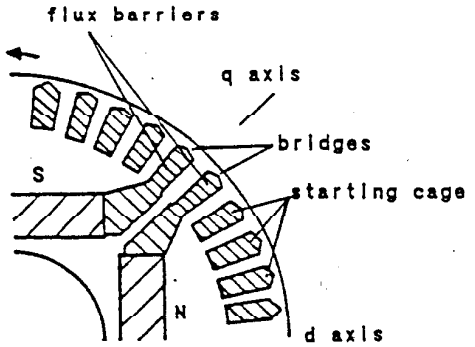

Fig. 1 One pole rotor cross section of a four pole, line start, buried magnet synchronous motor.

The additional harmonic field core loss is an important consideration when comparing motor steady state efficiency for constant speed line start applications. Buried magnet motors have also been proposed for use in variable speed drive applications [11-15] where the rotor starting cage may be eliminated in order to optimize the magnet geometry. In these applications the stator core loss is also an important consideration, especially at high speed, flux weakening operating conditions. As the speed increases the motor copper loss remains relatively constant due to inverter current limits while core loss may increase significantly due to the increased frequency of the fundamental component stator field.

In this paper the measured core loss characteristics of the line start motor pictured in Figure 1 will be presented and discussed. A method of predicting the stator core loss due to stator harmonic fields through the use of two dimensional finite element techniques will be presented. Finally a qualitative analysis of the origin of the stator harmonic fields for all types of buried magnet motors will be presented.

MEASURED POWER LOSS OF A LINE START MOTOR

The measured loss components of a 230 volt, two horsepower, buried magnet permanent magnet synchronous motor for 60 Hz operation at two loads and a range of voltages are shown in Figure 2. The rotor geometry of this motor was given in Figure 1 and its nameplate data is listed in Appendix A. The motor was operated from a sinusoidal line to line voltage source for all test conditions. Core loss was defined as the difference between the input power and the output power minus friction, windage and stator copper loss.

The I^2R loss exhibits a minimum for no load operation near the open circuit motor voltage as expected since above or below this voltage armature current must act to increase or decrease the air gap field. No load core loss also exhibits a minimum at the open circuit voltage as core loss begins to increase with decreasing voltage below this point. For the one horsepower operating condition minimum I^2R loss is obtained near rated voltage while measured core loss increases with decreasing voltage at low fundamental component flux levels. Obviously the motor core loss is not entirely due to fundamental component fields or the measured characteristics would show a minimum at zero voltage. At low voltage levels the core loss is highly dependent upon the motor load and the terminal voltage.

Further insight into the low voltage core loss phenomenon was gained by placing a full pitch search coil in the stator slot openings. Figure 3 contains plots of the measured search coil voltage at three terminal voltages for no load, 60 Hz operating conditions. The air gap field becomes more and more distorted as the terminal voltage is lowered even though the line to line voltage was purely

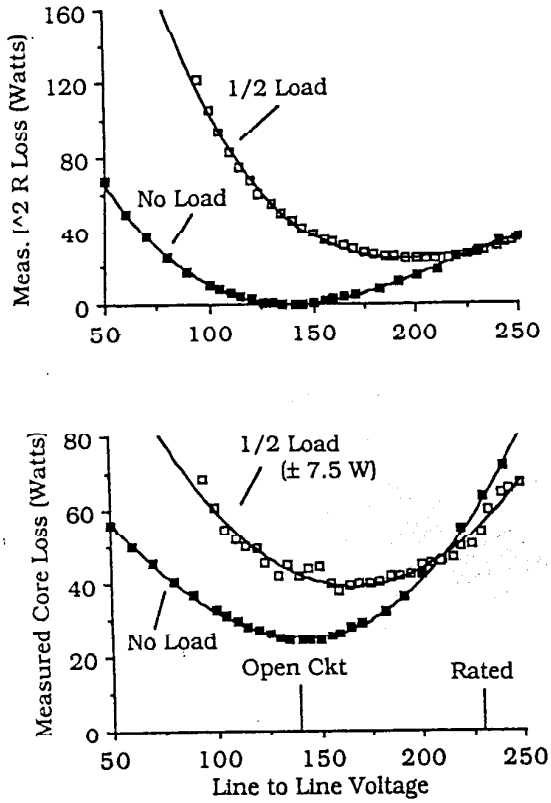

Fig. 2 Measured loss components of a two hp buried magnet synchronous motor for 60 Hz, sinusoidal terminal voltage.

sinusoidal. The third harmonic air gap field is especially noticeable in the 90 volt waveform. Harmonic analysis of the search coil voltage waveforms indicated that the third harmonic was larger than the fundamental component for no load terminal voltages below 90 volts. Harmonic analysis of the no load currents showed little harmonic distortion [16] indicating that additional field harmonics must either be induced by armature reaction and/or are a consequence of the permanent magnet air gap field.

The air gap harmonic fields will no doubt penetrate the stator core where they produce additional hysteresis and eddy current core loss especially at low voltage levels under rated speed conditions. Normal line start motor applications would operate the motor at rated voltage under steady state conditions where this additional loss is not important. For a buried magnet motor coupled to a variable frequency inverter, however, low air gap flux operating conditions are obtained when the drive enters its flux weakening mode of operation above base speed [11.14.15]. Here the additional core loss created by the stator harmonic fields may be a significant component of the total motor losses.

CALCULATION OF STEADY STATE STATOR CORE LOSS

It is difficult to quantify the effects of the induced harmonic air gap fields on stator core loss without detailed knowledge of the penetration of these fields into the stator core structure. A two dimensional finite element analysis magnetic field calculation program package was therefore utilized for calculating steady state stator harmonic fields in order to determine the stator core loss. The details of the calculation methods employed to obtain terminal voltage from input currents for this program package are described in [16]. Only the core loss calculation method will be breifly discussed here.

Finite element solutions in one pole of the permanent magnet motor cross section were obtained for each input set of stator d and q axis current components. (See Appendix C for dq axis orientation.) Constant speed operation was assumed for a fundamental armature current frequency of ω_e radians/second. The field distribution at several time instances in the fundamental current cycle was obtained by simultaneous rotation of the rotor grid and phase advancement of the stator currents. The rotor position was denoted by the electrical angle β as shown in Figure 4 with $\omega_e t = 0$ chosen as the point in time when the rotor q axis coincides with the a phase winding axis.

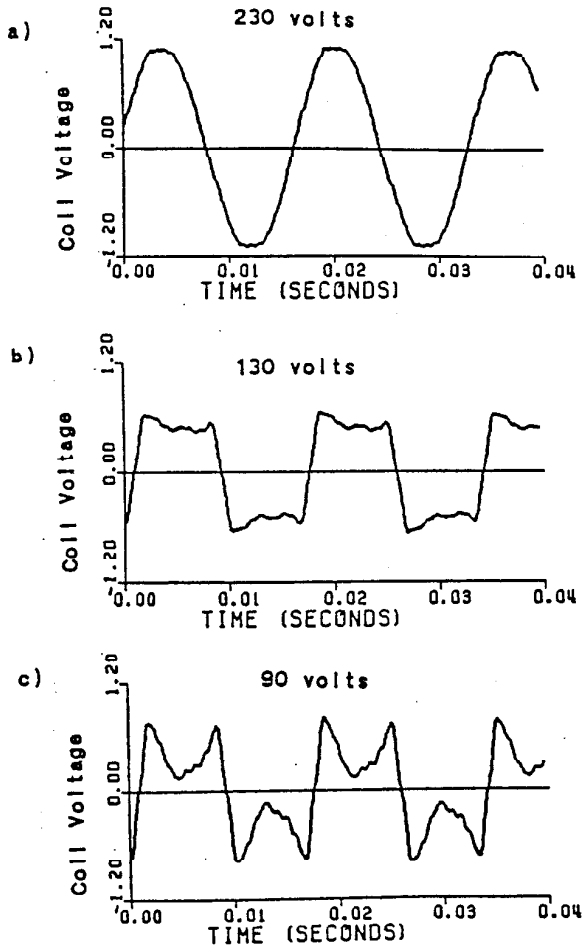

Fig. 3 Full pitch search coil voltage for no load operation of the buried magnet synchronous motor with sinusoidal terminal voltage.

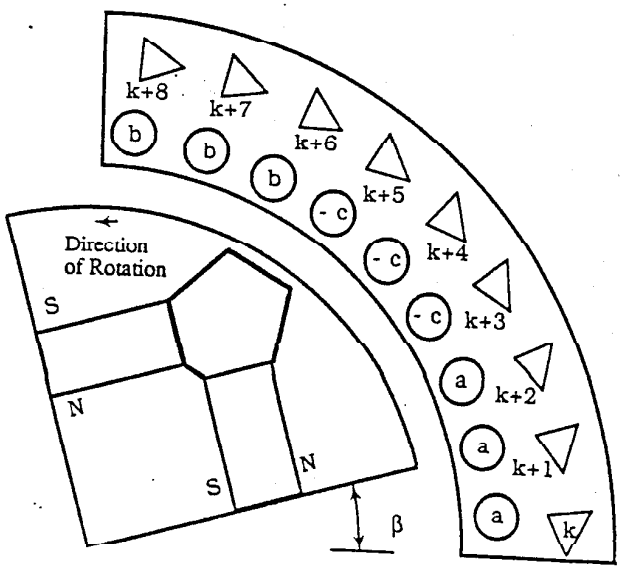

Fig. 4 Idealized one pole solution region for a four pole, 36 slot, unity pitch machine showing stator slot pitch elements.

Consider finite element k in Figure 4 lying in the first stator slot pitch of the one pole solution region. From a field solution with $\beta = 0$ the radial, B_{rk}, and circumferencial, B_{ck}, flux density at the element centroid is calculated for $\omega_e t = 5\pi/6$. The stator grid was generated by repeating the finite element pattern over each slot pitch so that in each slot pitch there is an element with the same area and in the same position as element k. These elements, k+1 through k+8, are illustrated in Figure 4. For balanced three phase armature currents containing only odd harmonics the following 1/6 period relationships exist between the abc currents:

$$-i_c(\omega_e t+\frac{\pi}{3}) = i_a(\omega_e t)\,,\; i_b(\omega_e t+\frac{\pi}{3}) = -i_c(\omega_e t)$$

$$\text{and } i_a(\omega_e t+\frac{\pi}{3}) = -i_b(\omega_e t). \qquad (1)$$

$$i_b(\omega_e t+\frac{2\pi}{3}) = i_a(\omega_e t),\; -i_c(\omega_e t+\frac{2\pi}{3}) = -i_b(\omega_e t)$$

$$\text{and } i_a(\omega_e t+\frac{2\pi}{3}) = i_c(\omega_e t). \qquad (2)$$

Combining the effects of (1) and (2) with the assumption of constant rotor speed the flux density values in the slot pitch elements from a single field solution can be used to obtain flux density components in element k at two other instants of time in a fundamental component half cycle. In particular, for a single field solution with $\beta = 0$ (i. e. $\omega_e t = 5\pi/6$) the radial flux density component in element k can be found from

$$B_{rk}(\omega_e t = \frac{5\pi}{6}+\frac{\pi}{3}) = -B_{rk+6}(\omega_e t = \frac{5\pi}{6})\,,$$

$$B_{rk}(\omega_e t = \frac{5\pi}{6}+\frac{2\pi}{3}) = -B_{rk+3}(\omega_e t = \frac{5\pi}{6}). \qquad (3)$$

The upcoming calculated results were obtained from four field solutions at rotor rotation angles (β's) equally spaced over zero to $\pi/3$ electrical radians so that in each stator core element the radial and circumferential flux density was calculated at the following 12 times in a half cycle:

$$\omega_e t = \frac{5\pi}{6}+\frac{(i-1)\pi}{3}+\frac{(j-1)\pi}{12}\;;\quad \begin{matrix} i = 1,2,3 \\ j = 1,2,3,4 \end{matrix} \qquad (4)$$

These 12 values and their 12 half wave symmetry counterparts were input to a digital Fourier transform routine in order to determine the coefficients in the following series approximations for element k flux density components:

$$B_{rk}(t) = \sum_{i=1}^{n_B} B_{rki}\cos(i(\omega_e t+\theta_{rki})),$$

$$B_{ck}(t) = \sum_{i=1}^{n_B} B_{cki}\cos(i(\omega_e t+\theta_{cki}))\,. \qquad (5)$$

The continuous time approximation to element k's flux density vector in the finite element solution plane is simply

$$\overline{B}_k(t) = \sum_{i=1}^{n_B}\overline{B}_{ki}(t) = B_{rk}(t)\,\hat{r} + B_{ck}(t)\,\hat{\theta}\,. \qquad (6)$$

This distorted rotational field was broken into two translational components by projecting $\overline{B}_k(t)$ onto the major and minor axes associated with the ellipse described by $\overline{B}_{k1}(t)$. The total core loss for element k was calculated as the sum of the loss associated with these two translational fields. The total core loss for a rotational field was shown to be accurately approximated by this sum for single frequency $\overline{B}(t)$ waveforms in [17]. The core loss associated with the major and minor axis element flux density translational magnetic fields was calculated from standard 60 Hz loss data combined with eddy current and hysteresis loss factors as described in [18]. The harmonic loss factors were derived from experimental loss data in [19] and take into account not only the harmonic content of the waveforms but also their waveshape and peak values since all three of these characteristics affect the level of core loss. See Appendix B for definitions of the loss factors obtained from [19]. The calculated core loss in all stator elements were added together to obtain the total stator core loss. Rotor core loss was neglected in the analysis.

A comparison of calculated and measured core loss characteristics for two load conditions and 60 Hz operation are given in Figure 5. Sinusoidal armature currents were assumed for the finite element model. Calculated stator core loss with seven flux density time harmonics included in the analysis (i. e. $n_B = 7$ in (5)) agrees quite well with measured data for both motor loads over a wide range of flux levels. Also plotted is the calculated stator core loss using only the fundamental component stator core flux density in each stator finite element ($n_B = 1$). Notice the large difference between the two calculated curves at low voltages for both loads where the effects of the stator field harmonics act to increase the core loss by up to a factor of six over that expected with only fundamental component fields. In a variable speed drive this low flux operating condition will be reached when the motor goes into a flux weakening mode at high speed.

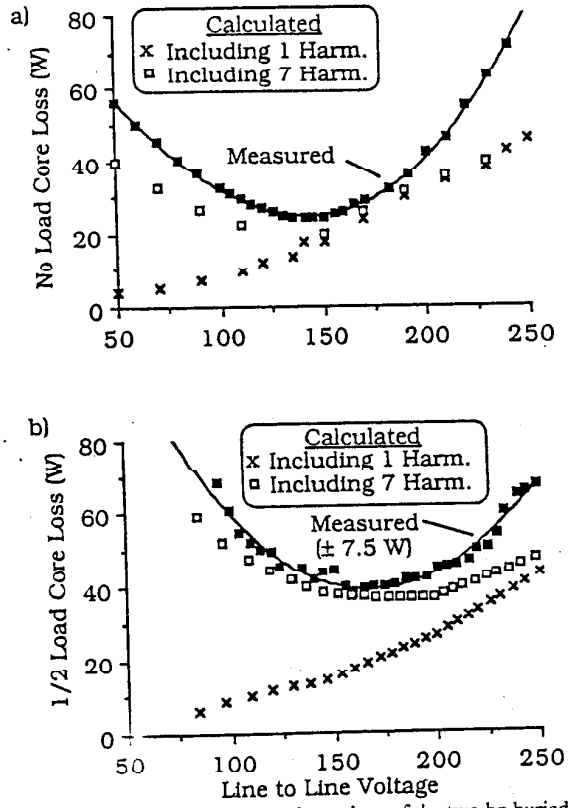

Fig. 5 Calculated and measured core loss of the two hp buried magnet synchronous motor for 60 Hz operation.

The additional harmonic core loss is especially evident in the one horsepower load, low voltage operating condition. Here the calculated stator flux density waveforms showed high levels of harmonic distortion. Figure 6 contains plots of calculated stator flux density waveforms for 1/2 load, 91 volt operation for a finite element located at the center of the tooth near the air gap. It can be noted that both field components contain high levels of harmonic distortion and that the total field is highly rotational in nature. The total core loss associated with this element would be calculated as the sum of the loss associated with two translational fields acting in the major and minor axes of the fundamental component of $\overline{B}(t)$. In general, it was found that the sum of all core loss associated with minor axis translational fields comprised about 10% of the total calculated loss for a wide range of operating conditions. It was also found that the third harmonic field was the most significant contributor to harmonic core loss [16] in this particular motor.

The calculated stator core loss distribution for the low voltage, 1/2 load, 60 Hz operating condition is shown in Figure 7. A majority of the core loss is concentrated in the stator teeth and near the air gap as expected.

ORIGIN OF THE STATOR HARMONIC FIELDS

The dramatic increase in harmonic field core loss with decreasing voltage is a consequence of the redistribution of air gap flux under low flux conditions. These effects can be qualitatively examined by considering the ideal relationship between motor air gap field components. Figure 8 shows idealized plots of air gap flux density components for the motor operating at 1/2 load, 60 Hz and 106 volts. In Figure 8a) the magnet field is represented as a square wave while the total field is represented as a sinusoidal function of the air gap space angle. The magnitude and phase of this latter curve can be determined from the fundamental component terminal voltage magnitude and angle. The difference between the idealized sinusoidal total field and the magnet field is the armature reaction field which is plotted in Figure 8b). This difference represents the necessary armature reaction flux density which must be created by armature currents if the total air gap flux density is to remain sinusoidal.

Figure 8c) is a pictoral representation of the rotor construction showing the rotor pole faces (excluding the cage) and the q axis flux barrier regions. The magnet leakage flux is restricted by the small q axis bridges above the flux barriers. The ideal armature reaction flux must exit the left pole face and enter the right pole face for this particular operating condition. This pole to pole armature reaction flux is restricted by the q axis flux barriers and the high permeability magnets so that a majority of the flux will attempt to pass through the q axis bridges in the same direction as the magnet leakage flux. The bridges will saturate so that some of the armature flux will find a lower reluctance path by leaking across the air gap to the stator tooth tips and back again at the right pole face. This pole to pole zigzag flux will distort the total air gap flux density distribution near the q axis. The net result is distortion of the air gap flux density waveform and an increase in time harmonic tooth flux density.

The additional stator harmonic field core loss was shown to decrease at high voltage levels. Consider the idealized air gap flux for the low harmonic loss, rated voltage, no load operating condition pictured in Figure 9. Now the armature reaction flux is in opposition to the magnet leakage flux in the rotor q axis bridges so that they will be pulled out of saturation. The armature reaction flux remains in the rotor iron so that the air gap field is sinusoidal (see Figure 3a)) and low levels of harmonc field core loss are obtained (see Figure 5a)).

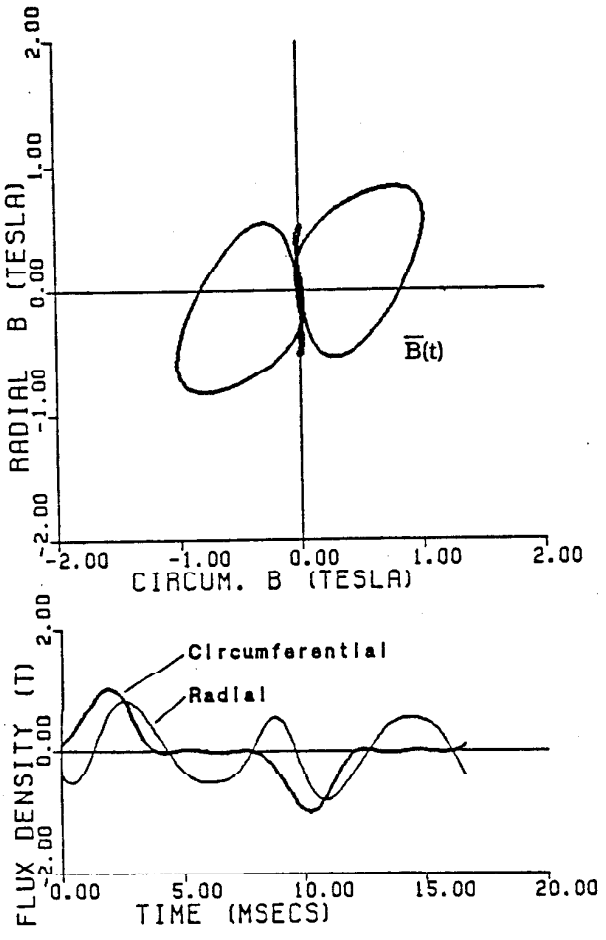

Fig. 6 Calculated flux density at the center of a stator tooth near the air gap for 1/2 load, 91 volt, 60 Hz operation.

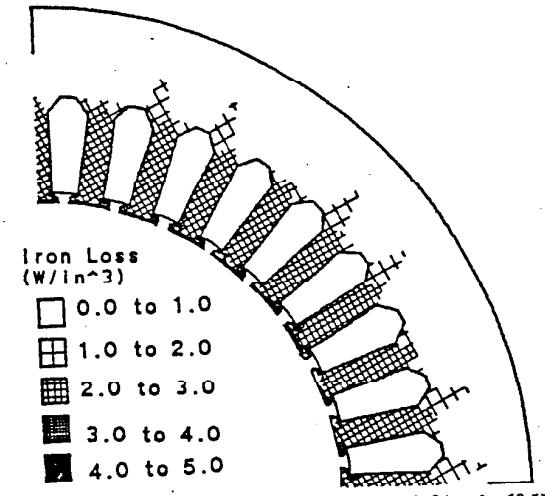

Fig. 7 Calculated stator core loss for 1/2 load, 91 volt, 60 Hz operation.

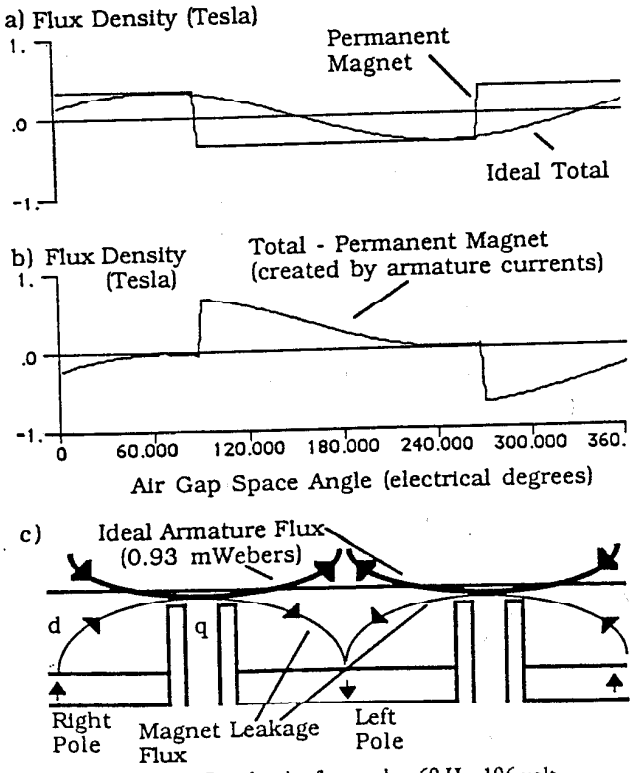

Fig. 8 Ideal air gap flux density for one hp, 60 Hz, 106 volt operation of the two hp buried magnet synchronous motor.

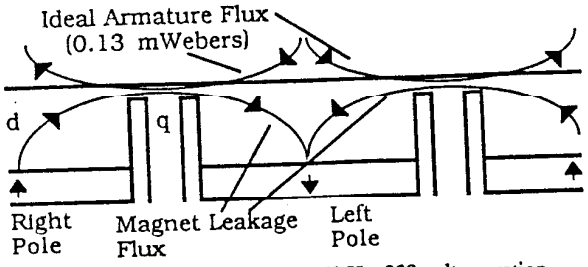

Fig. 9 Ideal air gap flux for no load, 60 Hz, 230 volt operation of the two hp buried magnet synchronous motor.

The harmonic core loss (difference between the calculated curves in Figure 5 a) and b)) should be directly related to the armature reaction pole to pole leakage flux and therefore to the armature current demagnetizing component ($-I_{ds}$ in Figure 12). Figure 10 shows a direct relationship between the harmonic core loss and I_{ds} for both the no load and 1/2 load operating conditions. The functional relationship between harmonic core loss and I_{ds} is saturation dependent so that different curves are expected for differing load (and I_{qs}) levels. For positive I_{ds} operating conditions the harmonic core loss is negligible since the armature reaction flux unsaturates the rotor q axis bridges.

The same localized rotor bridge saturation that effects stator field harmonics also causes the steady state magnetic characteristics of these types of motors to be highly nonlinear [8,11,12,16]. It is interesting to note that at low flux levels the buried magnet motor has stator harmonic fields which are due to iron saturation effects while at high flux levels they disappear. Usually core saturation affects field harmonics when the motor flux level is high. The importance of rotor leakage path saturation in the operation of this type of motor causes this relationship to be reversed.

The influence of I_{ds} on stator core loss extends over all motor operating conditions as shown in Figure 11 where calculated values of stator core loss are plotted against terminal voltage for five different I_{ds} values. At any given applied voltage the core loss increases with increasing demagnetizing armature current.

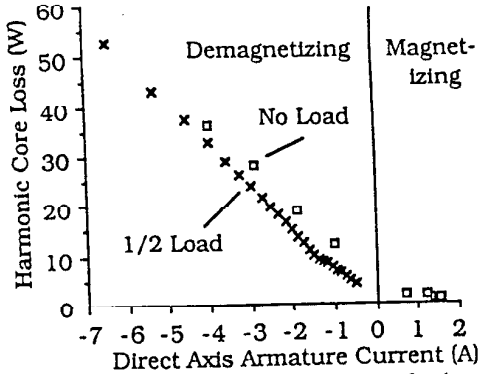

Fig. 10 Calculated stator harmonic core loss for the two hp motor.

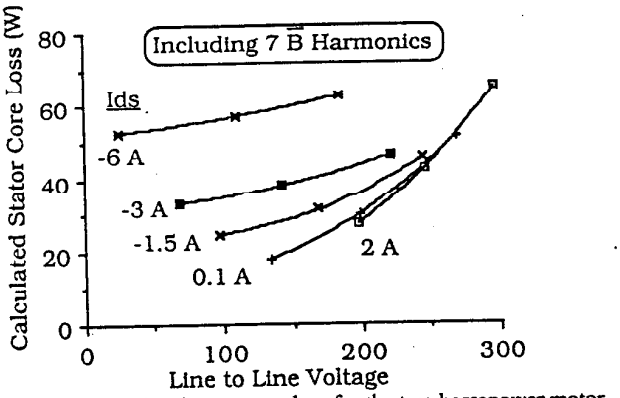

Fig. 11 Calculated stator core loss for the two horsepower motor.

CONCLUSIONS

The buried magnet synchronous motor was found to have significant levels of stator core loss due to harmonic fields at low motor flux levels. In some cases the harmonic fields acted to increase the core loss by a factor of six over that produced by the fundamental component field alone. It was shown that two dimensional finite element techniques could be used to accurately predict the stator core loss including the effects of waveform distortion in the stator core flux density. This calculation method proved to be a useful tool for evaluating the causes and effects of stator harmonic fields created by armature reaction.

The air gap field distortion is caused by localized saturation of rotor leakage flux paths which results in significant levels of pole to pole armature reaction zigzag flux at low flux levels (or high levels of demagnetizing armature current). The armature reaction field distortion is a direct consequence of the presence of rotor flux barriers to magnet leakage flux. These nonmagnetic barriers must always be present in order to drive a majority of the magnet flux across the air gap. Because of this, stator core harmonic fields should be expected for all buried magnet rotor synchronous motors (with or without a cage) when operating at low flux levels. This becomes increasingly important when these motors are operated in the high speed, low flux mode of operation in conjunction with a variable speed drive.

ACKNOWLEDGEMENTS

The authors wish to thank the industrial sponsors of the Wisconsin Electric Machines and Power Electronics Consortium (WEMPEC) for thier technical and financial support.

REFERENCES

1) Hanrahan, D. J. and D. S. Toffolo, "Permanent Magnet Generators, Part I - Theory," *AIEE Transactions*, December 1957, pp. 1098-1103.

2) Steen, C. R., "Direct Axis Aiding Permanent Magnets for a Laminated Synchronous Motor Rotor," *United States Patent*, #4,139,790, February 13, 1979.

3) Honsinger, V. "The Fields and Parameters of Interior Type AC Permanent Magnet Machines," *IEEE Transactions on Power Apparatus and Systems*, Vol. PAS-101, No. 4, April 1982, pp. 867-876.

4) Miller, T., T. W. Neumann and E. Richter, "A Permanent Magnet Excited High-Efficiency Synchronous Motor with Line-Start Capability," *IEEE Industry Applications Society Annual Meeting Conference Record*, 1983, pp. 455-461.

5) Richter, E. , T. Miller, T. Neumann and T. Hudson, "The Ferrite Permanent Magnet AC Motor - A Technical and Economic Assessment," *IEEE Transactions on Industry Applications*, Vol. IA-21, No. 4, May/June 1985, pp. 644-650.

6) Richter, E. and T. Neumann, "Line Start Permanent Magnet Motors With Different Materials," Paper AE-03 for the *INTERMAG Conference*, Hamburg, Germany, 1984.

7) Binns, K. J. and T. M. Wong, "Analysis and Performance of a High-Field Permanent Magnet Synchronous Machine," *IEE Proceedings*, Vol. 131, B, 6, November 1984, pp. 252-258.

8) Chalmers, B. J., S. K. Devgan, D. Howe and W. F. Low, "Synchronous Performance Prediction for High-Field Permanent Magnet Synchronous Motors," *Proceedings of the International Conference on Electrical Machines*, Munich, West Germany, September 1985, pp. 1067-1070.

9) Ishizaki, A., T. Tabako and K. Saitoh, "Prediction and Improvement on Synchronous Performance of AC Permanent Magnet Motor," *IEEE Industry Applications Society Annual Meeting Conference Record*, 1985, pp. 824-831.

10) Schiferl, R. F., R. S. Colby and D. W. Novotny, "Efficiency Considerations in Permanent Magnet Synchronous Motor Drives," *Electric Energy Conference (eecon-87) Conference Record*, Institute of Engineers, Australia, Adelaide, Australia, October, 1987, pp. 286-291.

11) Sneyers, B. ,D. W. Novotny and T. A. Lipo, "Field Weakening in Buried Magnet AC Motor Drives," *IEEE Transactions on Industry Applications*, Vol IA-21, No. 2, March/April 1985, pp. 398-407.

12) Consoli, A. and A. Abela, "Transient Performance of Permanent Magnet AC Motor Drives," *IEEE Transactions on Industry Applications*, Vol IA-22, No. 1, Jan/Feb 1986, pp. 32-41.
13) Chalmers, B. J., S. A. Hamad and G. D. Baines, "Parameters and Performance of a High-Field Permenant Magnet Synchronous Motor for Variable Frequency Operation," *IEE Proceedings*, Vol. 132, B, No. 3, May 1985, pp. 117-124.
14) Jahns, T. M., G. B. Kliman and T. W. Neumann, "Interior Permanent Magnet Synchronous Motors for Adjustable-Speed Drives," *IEEE Transactions on Industry Applications*, Vol. IA-22, No. 4, July/August 1986, pp. 738-747.
15) Jahns, T. M., "Flux-Weakening Regime Operation of an Interior Permanent Magnet Synchronous Motor Drive," *IEEE Transactions on Industry Applications*, Vol. IA-23, No. 4, July/August 1987, pp. 681-689.
16) Schiferl, R. *"Design Considerations for Salient Pole, Permanent Magnet Synchronous Motors in Variable Speed Drive Applications,"* Ph. D. Thesis, University of Wisconsin, Madison, Wisconsin, December 1987.
17) Yamaguchi, T. and K. Narita, "Rotational Power Loss in Commercial Silicon-Iron Laminations," *Electrical Engineering in Japan*, Vol. 96, No. 4, 1976, pp. 15-21.
18) Fouad, F. A., *"Finite Element Analysis for Design of Classical and Electronically Operated Machines,"* Ph. D. Thesis, Virginia Polytechnic Institute, Blacksburg, Virginia, May 1981.
19) Lavers, J. D., P. P. Biringer and H. Hollitscher, "A Simple Method of Estimating the Minor Loop Hysteresis Loss in Thin Laminations," *IEEE Transactions on Magnetics*, Vol. MAG-14, No. 5, September 1978, pp. 386-388.

APPENDIX A

Nameplate data of the buried magnet test motor: Three phase, two horsepower, 115/230 V,10.6/5.3 A, 60 Hz, 1800 rpm.

With the 230 volt connection: stator resistance = 1.15 Ω/phase and open circuit voltage @1800 rpm = 140 V.

Rotor magnets: Samarium Cobalt.

APPENDIX B: CORE LOSS CALCULATION

The core loss associated with a translational flux density waveform described by

$$B(t) = \sum_{i=1}^{n_B} B_i \cos(i(\omega_e t + \theta_i)) \qquad (7)$$

with peak flux density of B_p and with N flux reversals of magnitude ΔB_i per half cycle can be calculated as [19]

$$P_{core} = P_{e,sine}(B_p)^* K_e(B_i,B_p) + P_{h,sine}(B_p)^* K_h(B_p,\Delta B_i) \qquad (8)$$

where:

$P_{e,sine}(B_p)$ = eddy current loss for a fundamental component flux density with peak value B_p calculated using standard 60 Hz loss data,

$K_e(B_i,B_p)$ = correction factor for harmonic distortion:

$$= \left(\frac{B_i}{B_p}\right)^2 \sum_{i=1}^{n_B} \left(\frac{iB_i}{B_i}\right)^2 . \qquad (9)$$

$P_{h,sine}(B_p)$ = hysteresis loss for a fundamental component flux density with peak value B_p calculated using standard 60 Hz loss data,

and

$K_h(B_p,\Delta B_i)$ = correction factor for harmonic distortion

$$= 1 + \frac{0.65}{B_p} \sum_{i=1}^{N} \Delta B_i . \qquad (10)$$

APPENDIX C: D-Q REFERENCE FRAME

The direct (d) and quadrature (q) magnetic axes of the buried magnet permanent magnet rotor are aligned so that the d axis lies along the center of the magnet whose north pole faces the air gap and the q axis leads (wrt the direction of rotation) the d axis by 90 electrical degrees (see Figure 1). The corresponding direct and quadrature axis terminal voltage and current components are related to the terminal voltage phasors $\tilde{V}_s$ and $\tilde{I}_s$) as shown in Figure 12.

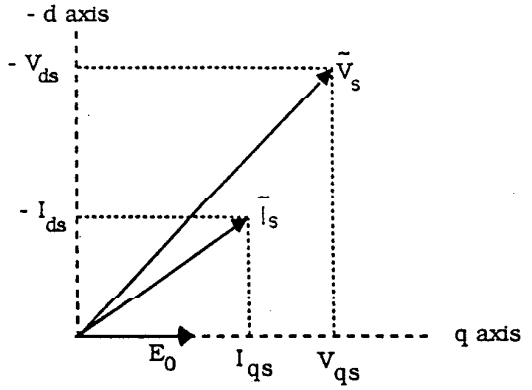

Fig. 12 D and q axis terminal voltage and current components.

Rich Schiferl (S-'80, M-'88) was born in Abbotsford, Wisconsin in 1958. He received his BSEE degree with high distinction from the University of Minnesota, Minneapolis in 1980, his MSEE degree from Purdue University, West Lafayette, Indiana in 1982 and his Ph. D. in Electrical Engineering from the Univeristy of Wisconsin, Madison in 1987. His Ph. D. research concerned the modelling and design of permanent magnet motors for variable frequency operation. Rich is currently an electrical development engineer at the Reliance Electric company in Cleveland, Ohio.

Thomas A. Lipo (M'64-SM'71-F'87) received his B.E.E. and M.S.E.E. degrees from Marquette University, Milwaukee, WI, in 1962 and 1964 respectively, and the Ph.D. degree in electrical engineering from the University of Wisconin in 1968.

From 1969 to 1979 he was an Electrical Engineer in the Power Electronics Laboratory of Corporate R&D, General Electric Co. He is presently a Professor in the Department of Electrical and Computer Engineering, University of Wisconsin-Madison. Dr. Lipo holds seven patents, has published over 75 papers and has received seven prize paper awards for his work. He is an active member of 5 IEEE Committees or Subcommitees and is past Chairman of two of them. He is a member of the Executive Board of the Industrial Applications Society and Editor of the IEEE Transactions on Power Electronics.